



HAL
open science

Microtubule acetylation but not detyrosination promotes focal adhesion dynamics and astrocyte migration

Bertille Bance, Shailaja Seetharaman, Cécile Leduc, Batiste Boëda, Sandrine Etienne-Manneville

► To cite this version:

Bertille Bance, Shailaja Seetharaman, Cécile Leduc, Batiste Boëda, Sandrine Etienne-Manneville. Microtubule acetylation but not detyrosination promotes focal adhesion dynamics and astrocyte migration. *Journal of Cell Science*, 2019, 132 (7), pp.jcs225805. 10.1242/jcs.225805 . pasteur-02118627

HAL Id: pasteur-02118627

<https://pasteur.hal.science/pasteur-02118627>

Submitted on 3 May 2019

HAL is a multi-disciplinary open access archive for the deposit and dissemination of scientific research documents, whether they are published or not. The documents may come from teaching and research institutions in France or abroad, or from public or private research centers.

L'archive ouverte pluridisciplinaire **HAL**, est destinée au dépôt et à la diffusion de documents scientifiques de niveau recherche, publiés ou non, émanant des établissements d'enseignement et de recherche français ou étrangers, des laboratoires publics ou privés.

SHORT REPORT

Microtubule acetylation but not deetyrosination promotes focal adhesion dynamics and astrocyte migration

Bertille Bance^{1,2,*}, Shailaja Seetharaman^{1,3,*}, Cécile Leduc¹, Batiste Boëda¹ and Sandrine Etienne-Manneville^{1,‡}

ABSTRACT

Microtubules play a crucial role in mesenchymal migration by controlling cell polarity and the turnover of cell adhesive structures on the extracellular matrix. The polarized functions of microtubules imply that microtubules are locally regulated. Here, we investigated the regulation and role of two major tubulin post-translational modifications, acetylation and deetyrosination, which have been associated with stable microtubules. Using primary astrocytes in a wound healing assay, we show that these tubulin modifications are independently regulated during cell polarization and differently affect cell migration. In contrast to microtubule deetyrosination, α TAT1 (ATAT1)-mediated microtubule acetylation increases in the vicinity of focal adhesions and promotes cell migration. We further demonstrate that α TAT1 increases focal adhesion turnover by promoting Rab6-positive vesicle fusion at focal adhesions. Our results highlight the specificity of microtubule post-translational modifications and bring new insight into the regulatory functions of tubulin acetylation.

This article has an associated First Person interview with the first author of the paper.

KEY WORDS: Microtubules, Adhesion, Migration, Post-translational modifications

INTRODUCTION

Cell migration relies on the polarization and coordinated regulation of cytoskeletal elements and adhesive structures (Lense and Etienne-Manneville, 2015; Wolfenson et al., 2009; Gardel et al., 2010; Parsons et al., 2010). While actin participates in the generation of forces that promote cell protrusion and cell net displacement, microtubules contribute to front-to-rear polarization (Elric and Etienne-Manneville, 2014; Etienne-Manneville, 2013) and focal adhesion (FA) dynamics (Stehbens and Wittmann, 2012; Etienne-Manneville, 2013). At the cell front, microtubules are captured in the vicinity of nascent adhesions and contribute to the polarized delivery of integrins towards these sites (Bretscher and Aguado-Velasco, 1998). Microtubules can also target FAs (Kaverina et al., 1998) and induce their disassembly through the recruitment of the endocytic machinery (Kaverina et al., 1999;

Kaverina et al., 2002; Palazzo et al., 2004; Ezratty et al., 2009; Stehbens et al., 2014). The polarized regulation of integrin-based structures implies that the functions of microtubules must be controlled in a polarized manner.

Several mechanisms, including MAP interactions and post-translational modifications of α - and β -tubulin (Janke, 2014; Song and Brady, 2015; Etienne-Manneville, 2010; Strzyz, 2016; Aillaud et al., 2016), affect microtubule dynamics or microtubule association with protein partners (Janke, 2014; Raunser and Gatsogiannis, 2015; Yu et al., 2015; Song and Brady, 2015). α TAT1 [also known as ATAT1, and as Mec-17 in *Caenorhabditis elegans* (Akella et al., 2010)] is the major tubulin acetyltransferase in mammals. It is responsible for the acetylation of the intraluminal lysine 40 of α -tubulin (Kalebic et al., 2013b). Deetyrosination is the elimination of the C-terminal tyrosine residue from α -tubulin by tubulin carboxypeptidase TCP (Aillaud et al., 2017). Tubulin tyrosine ligase (TTL) catalyses the reverse reaction on soluble tubulin. Lysine 40 acetylation and C-terminal deetyrosination of α -tubulin are both classically used as markers of stabilized microtubules, which are relatively long-lived and resistant to degradation. Both deetyrosinated and acetylated microtubules accumulate between the centrosome and the leading edge of migrating fibroblasts (Gundersen and Bulinski, 1988; Montagnac et al., 2013; Castro-Castro et al., 2012). However, the specific functions of deetyrosination and acetylation of microtubules are not well understood (Gadadhar et al., 2017; Song and Brady, 2015). α -Tubulin acetylation has been shown to facilitate fibroblast and neuronal motility (Hubbert et al., 2002; Creppe et al., 2009) but increased acetylation of microtubules can also reduce cell migration (Tran et al., 2007; Li and Yang, 2015). Using primary rat astrocytes, whose polarization and migration depend on microtubule dynamics (Etienne-Manneville, 2004; Etienne-Manneville and Hall, 2001), we analysed and compared the regulation and role of tubulin acetylation and deetyrosination. We found that these two modifications are independently regulated and that tubulin acetylation specifically impacts cell migration and increases FA turnover by promoting MICAL3-dependent fusion of Rab6A vesicles at FAs.

RESULTS AND DISCUSSION

Microtubule acetylation but not deetyrosination is upregulated during cell polarization and promotes cell migration

To determine how acetylation and deetyrosination are regulated during migration we quantified acetylated and deetyrosinated using antibodies specifically recognising deetyrosinated tubulin and K40-acetylated tubulin. In confluent astrocytes, acetylated and deetyrosinated microtubules are concentrated in the perinuclear region (Fig. 1A,B). Upon wounding, the proportion of acetylated tubulin increased while the proportion of deetyrosinated tubulin decreased. These changes were maximal 8 h after wounding when the cells migrate at a steady state (Fig. 1A,B; Fig. S1A). The decrease in

¹Cell Polarity, Migration and Cancer Unit, Institut Pasteur, UMR3691 CNRS, Equipe Labellisée Ligue Contre le Cancer, F-75015 Paris, France. ²Sorbonne Université, Collège doctoral, F-75005 Paris, France. ³Université Paris Descartes, Sorbonne Paris Cité, F-75006 Paris, France.

*These authors contributed equally to this work

‡Author for correspondence (setienne@pasteur.fr)

© S.S., 0000-0002-5151-7726; C.L., 0000-0002-1806-4120; S.E.-M., 0000-0001-6651-3675

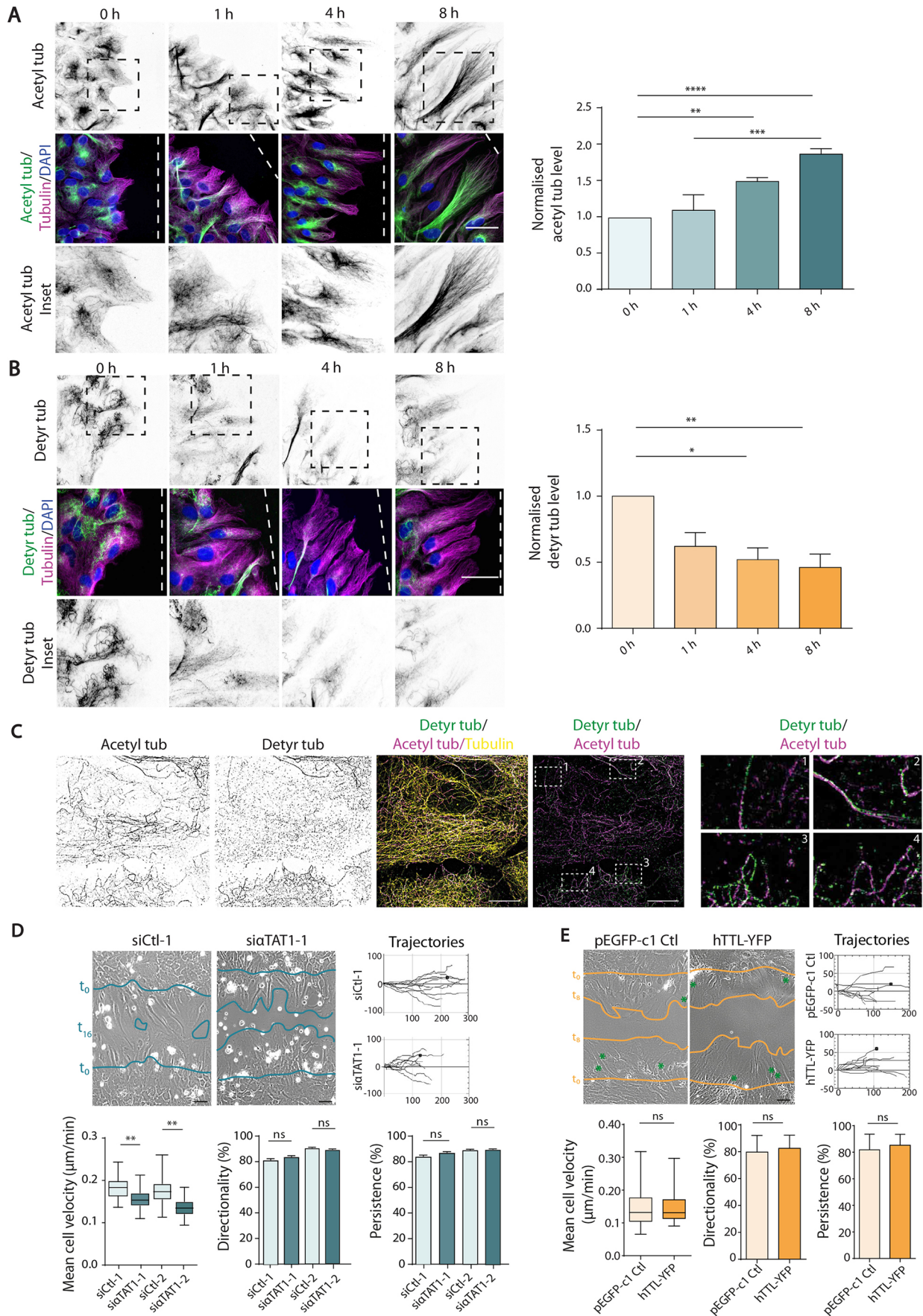


Fig. 1. See next page for legend.

Fig. 1. Microtubule acetylation but not deetyrosination increases during wound-induced migration and promotes cell migration. (A,B) Astrocytes were stained with antibodies against α -tubulin, acetylated tubulin (Acetyl tub) (A) or deetyrosinated tubulin (Detyr tub) (B) at indicated time points following wounding. Dashed lines indicate the wound orientation. Scale bars: 50 μ m. Graphs show the mean \pm s.e.m. normalized acetyl or deetyrosinated tubulin intensities for each condition (for acetyl levels, $n \geq 286$ cells/condition; for deetyrosinated tubulin levels, $n \geq 128$ cells/condition; $N=3$). (C) Super-resolution images showing non-migrating astrocytes stained for deetyrosinated tubulin (green), acetylated tubulin (magenta) and α -tubulin (yellow). White dashed boxes show regions of the zooms (on the right). Scale bar: 10 μ m. (D) Upper left panels show phase-contrast images of astrocytes transfected with indicated siRNAs. Blue lines indicate the wound edge immediately (t_0) or 16 h (t_{16}) after wounding. Scale bars: 100 μ m. Upper right panels show trajectories of 10 cells each from samples transfected with siCt1-1 or si α TAT1-1. The box-and-whisker plot (bottom left) shows the cell velocity (μ m/min). Histograms bottom right show mean \pm s.e.m. directionality (%) and persistence (%) of migrating astrocytes ($n \geq 70$ cells, $N=3$). (E) Upper left panels show phase-contrast images of migrating astrocytes expressing pEGFP-c1 or hTTL-YFP. Orange lines indicate the wound edge immediately (t_0) or 16 h (t_{16}) after wounding. Scale bar: 50 μ m. Upper right panels show trajectories of 10 cells each from cells expressing pEGFP-c1 and hTTL-YFP. The box-and-whisker plot (bottom left) shows the cell velocity (μ m/min). Histograms bottom right show mean \pm s.e.m. directionality (%) and persistence (%) of migrating astrocytes ($n \geq 70$ cells, $N=3$).

microtubule deetyrosination differs from what has been observed during wound-induced fibroblast migration (Gundersen and Bulinski, 1988). However, following wounding, fibroblasts require stimulation by serum or LPA to migrate, both previously shown to promote microtubule deetyrosination (Cook et al., 1998). In astrocyte wound healing assays, migration results solely from the wound and does not require addition of serum or LPA (Etienne-Manneville, 2006). When serum-starved rat embryonic astrocytes were submitted to a wound healing assay in serum-free conditions, similar increase in the levels of acetylated tubulin and decrease in deetyrosinated tubulin were observed (Fig. S1B). Using structure illumination based super-resolution microscopy, we observed that tubulin acetylation and deetyrosination were frequently found on the same microtubules but did not always colocalise, often decorating distinct microtubule regions (Fig. 1C).

To determine the role of microtubule acetylation on cell migration, we used two distinct sets of two siRNAs to inhibit α TAT1 expression in astrocytes. α TAT1 depletion strongly decreased microtubule acetylation (Fig. S1C) without modifying deetyrosinated tubulin level (Fig. S1D). Cell treatment with tubacin, a specific HDAC6 inhibitor (Haggarty et al., 2003) dramatically increased microtubule acetylation without affecting deetyrosination (Fig. S1D). α TAT1 depletion decreased cell migration speed but did not affect the direction or the persistence of migration (Fig. 1D; Movie 1). The polarized shape of wound edge cells was not perturbed by the reduction of acetylated microtubules (Fig. S1C; Movie 1).

To assess the specific role of deetyrosination in comparison with acetylation, we decreased deetyrosinated tubulin by overexpressing human TTL in rat embryonic astrocytes (Fig. S1E). Tracking of TTL-YFP-expressing cells showed that tubulin deetyrosination does not perturb cell migration speed, direction nor persistence (Fig. 1E; Movie 2). Taken together, our results indicate that microtubule deetyrosination and acetylation are independently regulated and have distinct roles during cell migration.

Microtubule acetylation but not deetyrosination affects FAs

Since microtubules are crucial for the control of cell adhesion, we investigated the impact of microtubule acetylation and deetyrosination on FAs. Depletion of α TAT1 did not modify the FA size but it changed the number and the localisation of FAs

(Fig. 2A,B). In control migrating cells, FAs were restricted to the front of the protrusion of wound edge cells, whereas in α TAT1-depleted cells FAs were visible throughout the basal surface. This resulted in an increased mean distance between FAs and the cell leading edge without modifying the spreading area and length of the cells (Fig. 2B; Fig. S2A). Expression of a siRNA-resistant α TAT1 construct rescued the number and distribution of FAs whereas a construct encoding a catalytically inactive form of α TAT1 (GFP- α TAT1-D157N) did not (Fig. 2A,B). In contrast to acetylation, reducing microtubule deetyrosination did not affect FA number, size or distribution (Fig. 2C,D), showing that microtubule acetylation, but not deetyrosination, affects FAs.

We then used GFP-paxillin-expressing astrocytes to analyse FA dynamics (Digman et al., 2008; Webb et al., 2004). α TAT1 depletion increased the FA lifetime as compared to control cells (Fig. 2E; Movie 3). In control astrocytes, FA dynamics was composed of two steps: assembly and disassembly (Gardel et al., 2010) (Fig. 2F,G). Decreased microtubule acetylation was associated with longer assembly and disassembly phases separated by a phase during which the size of FAs plateaued (Fig. 2F,G). In agreement with the wider distribution of FAs in α TAT1-depleted cells, the distance to the leading edge of assembling and disassembling FAs was increased in α TAT1-depleted cells (Fig. 2H). Altogether, these results show that the tubulin acetylase α TAT1 specifically controls FA number, distribution and dynamics.

Acetylated microtubules and α TAT1 localize at FAs

The impact of α TAT1 on FA dynamics led us to further investigate the localization of α TAT1 and acetylated microtubules. Cell wounding increased microtubule acetylation in the perinuclear region and at the front of migrating cells (Fig. 3A,B). There, stretches of acetylated tubulin were concentrated on microtubules in proximity to FAs while they appear less abundant in regions without FAs (Fig. 3C).

Since an anti- α TAT1 antibody did not allow us to visualize the endogenous protein in fixed cells, we used ectopic expression of GFP- α TAT1 to determine the localization of α TAT1. Expression of GFP- α TAT1 alone did not alter FA number nor distribution (Fig. S2B) but it rescued FAs numbers in α TAT1-depleted cells (Fig. 2A,B), suggesting that it behaves like the endogenous protein. GFP- α TAT1 was present on most microtubules, although different levels depending on the microtubule or the microtubule region (Fig. 3D; Movie 4). GFP- α TAT1-positive microtubules were also visible in proximity to FAs in mCherry-paxillin expressing cells (Fig. 3E). In some cases, GFP- α TAT1 also appears as straight dashes reminiscent of FAs and tips of stress fibres (see bottom right of the first panel in Fig. 3E). We thus used TIRF microscopy to closely visualise FAs and associated structures at the basal surface of cells, which revealed an accumulation of GFP- α TAT1 in mCherry-paxillin-positive FAs (Fig. 3F; Movie 5). These observations suggest that α TAT1 localizes at FAs and can locally promote acetylation of microtubules. The regulation of α TAT1 localization and/or activity during migration remains to be elucidated but may involve integrin signalling (Palazzo et al., 2004) or α TAT1 interaction with clathrin-coated pits localized around FAs (Montagnac et al., 2013).

α TAT1 controls Rab6 vesicle fusion at FAs

Microtubules can control FA dynamics through vesicular traffic (Ezratty et al., 2009; Ezratty et al., 2005; Shafaq-Zadah et al., 2016). The small GTPase Rab6 that decorates most post-Golgi carriers (Fourriere et al., 2018 preprint) has been involved together with Rab8 in vesicular traffic to FAs (Stehbens et al., 2014; Grigoriev et al.,

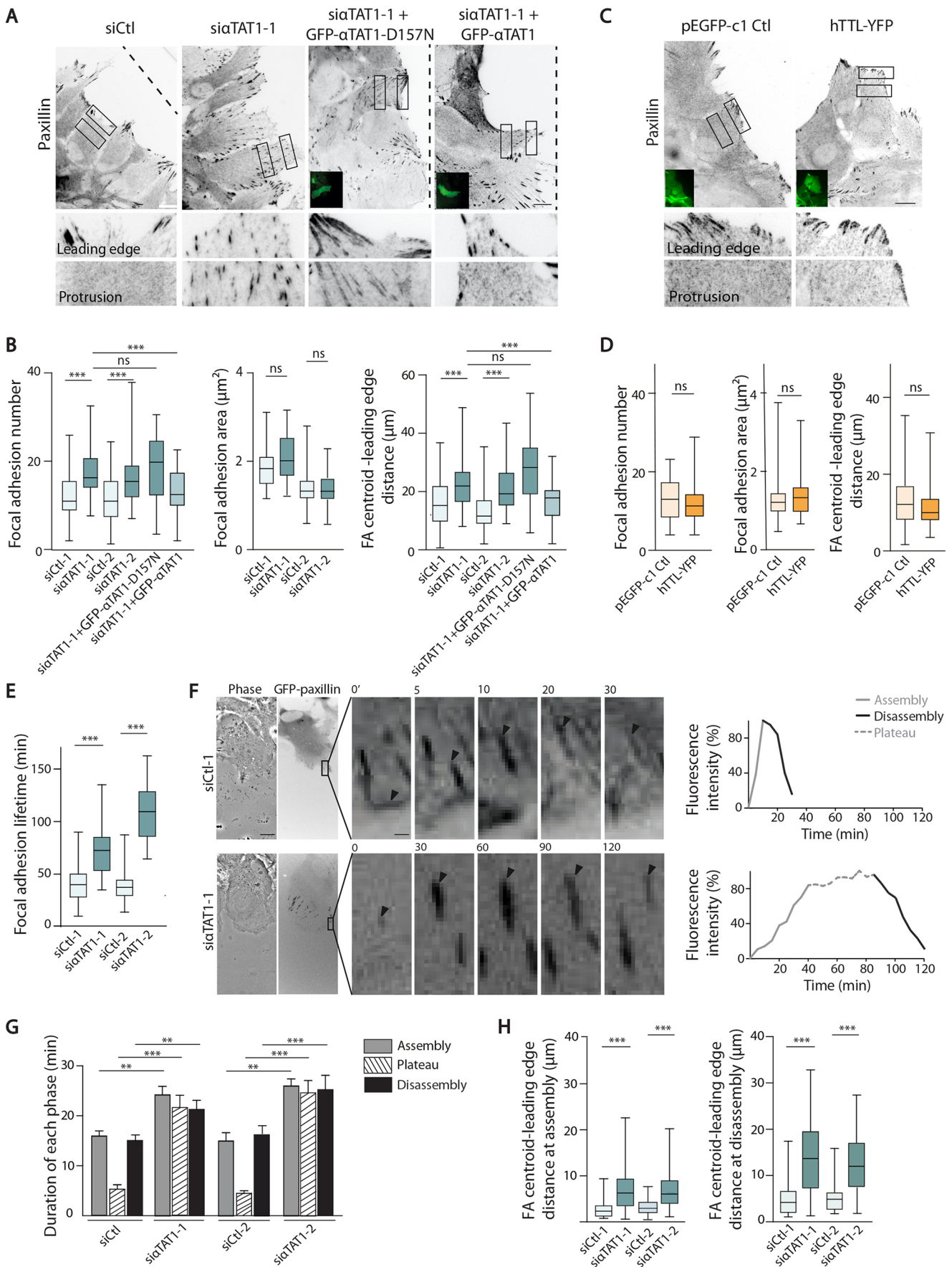


Fig. 2. See next page for legend.

Fig. 2. Microtubule acetylation but not detyrosination controls focal adhesions. (A,C) Epifluorescence images of paxillin immunostaining (inverted contrast) in migrating (8 h after wounding) astrocytes transfected with the indicated siRNAs and/or plasmids (insets show GFP expression). Dashed lines indicate the wound orientation. Scale bar: 10 μ m. The bottom panels correspond to the zooms of the boxed regions located at the leading edge or further back within the protrusions. (B,D) Box-and-whisker plots showing the number, area (μ m²) and distance leading edge (μ m) of FAs in migrating astrocytes transfected with indicated siRNAs and plasmids ($N > 3$, 100 cells per conditions/per experiment), as shown in A,C. (E) Box-and-whisker plot showing the FA lifetime in migrating astrocytes transfected with GFP-paxillin and indicated siRNAs ($N = 3$; 10 FA per cell; 10 cells per condition). (F) The two left panels show the phase-contrast and fluorescence (inverted contrast) images of migrating astrocytes expressing GFP-paxillin (as shown in Movie 2). Scale bar: 15 μ m. Higher magnification images to the right show the dynamics of FAs located in the region indicated by the black box in the GFP-paxillin panel. Scale bar: 1.5 μ m. Real time (in min) is indicated in the top left corners. Graphs show the fluorescence intensity (as a percentage of the maximum intensity) over time of one FA (black arrowhead) per treatment. (G) Histogram showing mean \pm s.e.m. ($N = 3$, 5 FA per cell, 10 cells per condition) duration of each phase of FA dynamics. (H) Box-and-whisker plots showing distance between FA centroid and leading edge during the FA assembly and disassembly ($N > 3$, 100 cells per conditions per experiment).

2007). To assess the impact of α TAT1 on Rab6A-positive vesicle trafficking to FAs, we expressed GFP-Rab6A in control or α TAT1-depleted astrocytes. GFP-Rab6A associated with the Golgi complex and cytoplasmic vesicles as described in other cell types (Goud et al., 1994) (Movie 6). We did not detect any effect of microtubule acetylation on the presence of Rab6-positive vesicles on microtubules (Fig. S3A). Using mCherry-paxillin-expressing cells, we observed that GFP-Rab6A-positive vesicles were transported towards FAs where the fluorescence disappeared, indicating vesicle fusion with the plasma membrane (Fig. 4A,B; Movie 6) (Grigoriev et al., 2011). Kymograph analysis showed that in control cells GFP-Rab6A-positive vesicles underwent rapid docking followed by fusion. In contrast, GFP-Rab6A-positive vesicles in α TAT1-depleted cells reached FAs but the number of fusion events was strongly decreased (Fig. 4A,B). Furthermore, when fusion occurred in α TAT1-depleted cells, the time between immobilization and fusion with the plasma membrane was strongly increased (Fig. 4C). The fusion of Rab6A-positive vesicles has been shown to be promoted by Rab6 and Rab8 interaction with the flavoprotein monooxygenase MICAL3 and the cortical factor ELKS (also known as ERC1) at the periphery of FAs (Grigoriev et al., 2011). When expressed in astrocytes, GFP-ELKS (Fig. 4D) and GFP-MICAL3 (Fig. 4E) clearly decorated the periphery of FAs as previously reported (Grigoriev et al., 2011). Although α TAT1 depletion did not perturb ELKS localization around FAs, it led to a strong decrease in MICAL3 recruitment at the periphery of FAs (Fig. 4F,G), suggesting that microtubule acetylation does not directly affect the recruitment and transport of Rab6-positive vesicles on microtubules but instead facilitates vesicle fusion at the plasma membrane by participating in the recruitment of MICAL3 in the vicinity of FAs. We then used siRNA to specifically downregulate of Rab6A and MICAL3 (Fig. S3B,C) to determine whether alteration of Rab6-dependent traffic and MICAL3-dependent fusion of Rab6-positive vesicles could participate in the control of FA dynamics. Both Rab6A depletion and MICAL3 depletion increased the number of FAs and altered their distribution in a manner similar to that observed in α TAT1-depleted cells (Fig. S3D,E) without affecting microtubule acetylation (Fig. S3F). Taken together, these observations strongly suggest that α TAT1-mediated microtubule acetylation facilitates MICAL3-dependent fusion of Rab6A-positive vesicles to promote FA dynamics.

Our results highlight the specific regulation and role of microtubule acetylation and detyrosination during cell migration. The fact that detyrosination and acetylation during astrocyte migration are differently regulated and can decorate distinct microtubule regions strongly suggests that these two modifications, often considered as equivalent markers of stable microtubules are, in fact, unique. Moreover, microtubule acetylation, but not detyrosination, is associated with faster FA turnover and cell migration. So far, α TAT1 is the only acetyl transferase known to induce tubulin acetylation at lysine 40, and no other substrates of α TAT1 are known. Since α TAT1 depletion induced a decrease of microtubule acetylation, our results strongly suggest that α TAT1 functions are mediated by acetylated microtubules. However, we cannot completely exclude the possibility that α TAT1 also acts through an alternative mechanism. α TAT1 has been shown to destabilize microtubules independently of its acetyltransferase activity (Kalebic et al., 2013a) and its interaction with proteins such as doublecortin (also known as DCLK1) or cortactin (also known as CTTN) may be involved (Kim et al., 2013; Castro-Castro et al., 2012). Nevertheless, the effects of α TAT1 depletion on FA turnover were rescued by ectopic expression of α TAT1-WT but not by the catalytically inactive mutant, confirming acetylation by α TAT1 as crucial to its function in cell adhesion and migration. Inhibition of HDAC6 with tubacin to induce the hyperacetylation of microtubules inhibited cell migration (Fig. S3G). This may be explained by the fact that HDAC6, in contrast with α TAT1, has a large number of substrates (Zhang et al., 2007; Gao et al., 2007; Kovacs et al., 2005) through which it affects actin dynamics, macropinocytosis as well as FA turnover and cell migration (Akella et al., 2010; Kim et al., 2013). Rab6A controls the transport and fusion of secretory carriers (Grigoriev et al., 2007; Grigoriev et al., 2011) and we can hypothesise that it contributes to the trafficking of essential components towards the forming FAs, which may explain the slower assembly of FAs in the absence of α TAT1. Rab6A has also been identified as being involved in the retrograde transport of integrins during cell migration (Shafaq-Zadah et al., 2016), suggesting that microtubule acetylation may also affect FA dynamics by controlling integrin recycling.

In conclusion, our results demonstrate the specificity of microtubule acetylation and detyrosination, two post-translational modifications identically used at markers of stable, long-lived microtubules. We also show here that microtubule acetylation plays a crucial role in the control of vesicular traffic, FA dynamics and ultimately controls cell migration speed.

MATERIALS AND METHODS

Cell culture

Primary astrocytes were obtained from E17 rat embryos (Charles River Laboratories) using the procedure detailed in Etienne-Manneville (2006), according to the guidelines approved by the French Ministry of Agriculture and following European standards. Astrocytes were grown in 1 g/l glucose DMEM supplemented with 10% FBS (Invitrogen), 1% penicillin-streptomycin (Gibco) and 1% Amphotericin B (Gibco) at 5% CO₂ and 37°C.

Transfection

Astrocytes were transfected with Lonza Basic Nucleofector glial transfection solution and electroporated with a Nucleofector machine (Lonza). Cells were then plated on appropriate supports previously coated with poly-L-ornithine (Sigma). Experiments were carried out 3 or 4 days post-transfection and comparable protein silencing was observed. siRNAs were used at 1 nmol for astrocytes. siRNA sequences used were: Luciferase (control), UAAGGCUAUGAAGAGAUAC; α TAT1 rat (si α TAT1-1), 5'-ACCGACACGUUUUAUGU-3' and 5'-UUCGAAACCGCAGGAA-CG-3'; α TAT1 rat (si α TAT1-2), 5'-UAAUGGAUGUACUCAUCA-3'

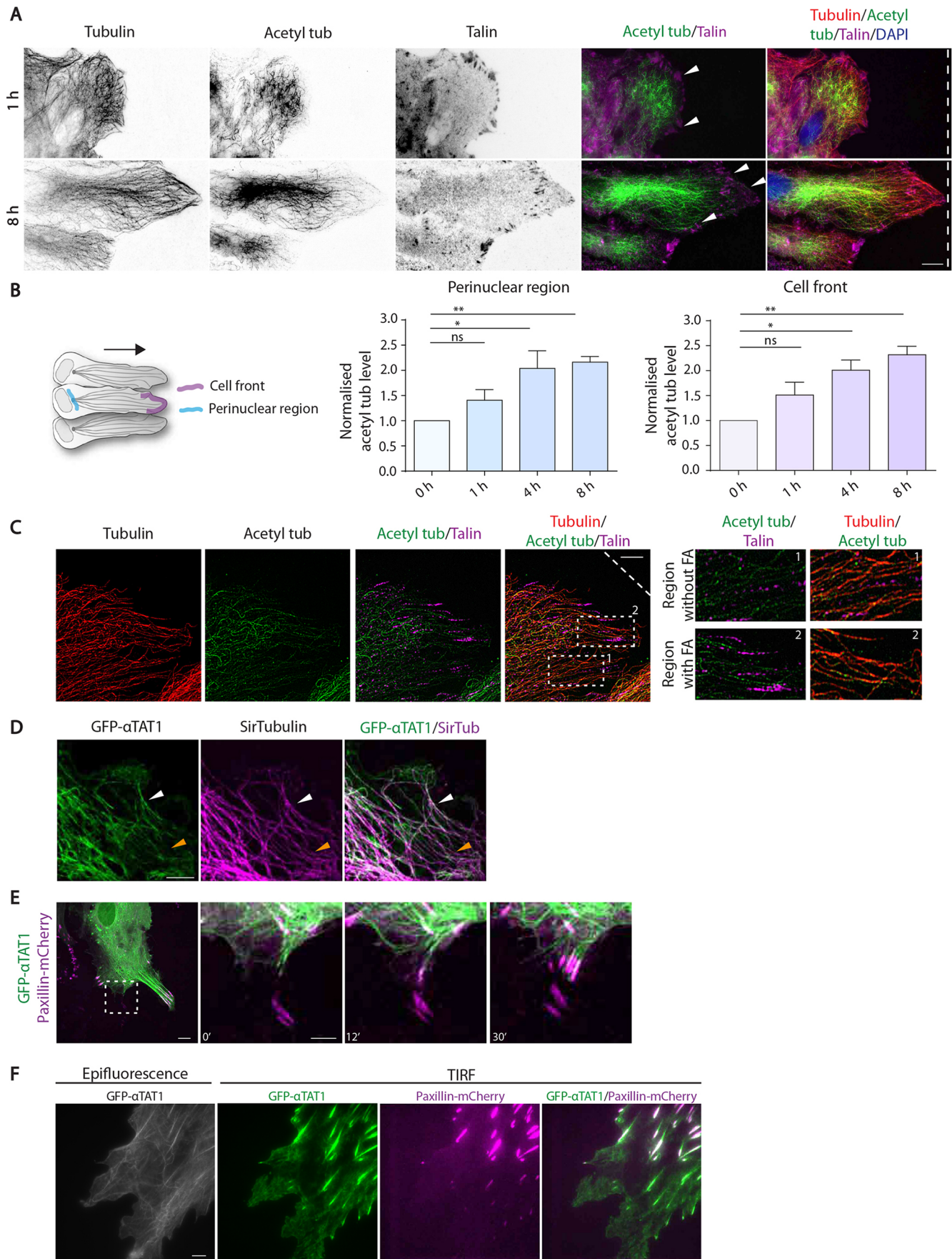


Fig. 3. See next page for legend.

Fig. 3. Acetylated microtubules and α TAT1 acetyltransferase localize at focal adhesions. (A) Migrating astrocytes immunostained with α -tubulin (inverted contrast and red), acetylated-tubulin (inverted contrast and green) and talin (inverted contrast and magenta) 1 h and 8 h after wounding. Dashed lines indicate wound orientation and white arrowheads point to the regions of interest. (B) Graphs showing mean \pm s.e.m. of the normalized ratios of acetylated tubulin over total tubulin at the cell front (purple) or perinuclear region (blue). The left schematic illustrates these different regions (perinuclear levels, $n \geq 62$ cells; cell front levels, $n \geq 167$ cells; $N=3$). (C) Super-resolution images of α -tubulin (red), acetylated-tubulin (green) and talin (magenta) immunostaining of a migrating astrocyte 8 h after wounding. Boxed regions are magnified in panels to the right. (D) Migrating astrocytes (6 h after wounding) expressing GFP- α TAT1 (green) and treated with SirTubulin (magenta) 1 h prior to acquisition. White arrowheads indicate regions where α TAT1 overlaps with microtubules and orange arrowheads indicate regions with minimal α TAT1 on microtubules. (E) Fluorescence images of astrocyte expressing GFP- α TAT1 (green) and mCherry-paxillin (magenta) 6 h after wounding. Higher-magnification images (right) show the region in the left-hand panel indicated by a white dashed box, at different time points of Movie 5. (F) Epifluorescence (left) and TIRF images (right) of astrocyte expressing GFP- α TAT1 (grey or green) and mCherry-paxillin (magenta) 6 h after wounding. Scale bars: 10 μ m in A, 5 μ m in C–F.

and 5'-UCAUGACUAUUGUAGAUGA-3'; Rab6A rat, 5'-GCAACAAUUGGCAUUGACUUCUUUAU-3' and 5'-CAAACAAUCCAGCAUAUCUGGUAU-3'.

DNA plasmids used were: pEGFP (Clontech), pEGFP-paxillin (from Ana-Maria Vallés, Institut Curie, Paris, France), pPaxillin-mCherry cloned from pPaxillin psmOrange with BamHI and NotI, hTTL-GFP (human; from Carsten Janke, Institut Curie, Orsay, France), EGFP-Rab6A (human; from Bruno Goud, Institut Curie, Paris, France), mEB3-FL pEGFP-N1 (gift from Nathalie Morin, CRBM, Montpellier, France), EGFP- α TAT1 and GFP- α TAT1-D157N (from Philippe Chavrier, Institut Curie, Paris, France), GFP-MICAL3 and GFP-ELKS (gift from Anna Akhmanova, Utrecht University, The Netherlands).

2D wound healing assay

Cells were plated on appropriate supports (dishes, plates, coverslips or glass-bottom MatTek dishes). Cells were allowed to grow to confluence and fresh medium was added the day prior to the experiment. The cell monolayer was then scratched with a p200 pipette tip to induce migration.

Immunofluorescence

Cells migrated for 8 h (unless otherwise stated), and were then fixed with cold methanol for 3–5 min at -20°C or 4% warm PFA for 10 min and permeabilised for 10 min with Triton X-100 0.1%. Coverslips were blocked for 30 min with 5% BSA in PBS. The same solution was used for primary and secondary antibody incubation for 1 h. Nuclei were stained with DAPI or Hoechst 33342 and were mounted with Prolong Gold with DAPI (Life Technologies). Epifluorescence images were acquired with a Leica DM6000 microscope equipped with 40×1.25 NA or 63×1.4 NA objectives and recorded on a CCD camera with Leica software. Super-resolution 3D-SIM images were acquired with a Zeiss LSM780 ELYRA with 63×1.4 NA or 100×1.46 NA objectives and recorded on an EMCCD camera Andor Ixon 887 1K with Zen software.

Antibodies used in this study are anti-acetylated tubulin (1:7500, clone 6-11B-1, Sigma), anti-Poly-Glu tubulin (1:1000, AbC0101, ValBiotech), anti- α -tubulin (1:500, MCA77G, Bio-Rad), anti-GFP-FITC (1:1000, ab6662, Abcam), anti-Paxillin (1:1000, 610051, mouse monoclonal, BD Transduction; and ab32084, rabbit monoclonal, clone Y133, Abcam), anti-Talin (1:1000, T3287, Sigma-Aldrich), anti-APC (gift from Inke Nathke, University of Dundee, Dundee, UK) and anti-Rab6 (gift from Bruno Goud, Institut Curie, Paris, France). Since the paxillin staining was not compatible with methanol fixation, anti-talin antibodies were used to co-stain FAs and microtubules. For live experiments, microtubules were fluorescently labelled with Sir-Tub (Cytoskeleton, 1/2500 of a 50 μ M stock 1 h prior image acquisition), and treated with Niltubacin (Enzo Life Sciences) or tubacin (Sigma-Aldrich) added prior to wounding.

Live imaging

For phase-contrast wound healing assays, cells in 12-well plates were wounded with a p200 pipette tip and directly placed in the microscope with the addition of HEPES and paraffin to eliminate medium evaporation. Image acquisition was launched about 30 min after wounding. Movies were acquired with a Zeiss Axiovert 200M equipped with a thermostatic humid chamber with 5% CO_2 and 37°C . Images were acquired every 15 min for 24 h, with dry objective 10×0.45 NA and an EMCCD or sCMOS pco edge camera.

For fluorescence live imaging, cells on appropriate dishes (MatTek) were wounded and allowed to migrate 4 h before image acquisition. HEPES and antioxidants were added to the medium before acquisition. Epifluorescence experiments investigating paxillin turnover were performed with a Nikon BioStation IM-Q ($40\times$ objective) at a rate of 1 frame/5 min for 3–5 h with 5% CO_2 and 37°C . Confocal experiments were performed on a Perkin-Elmer spinning disk confocal microscope equipped with an EMCCD camera and a 63×1.4 NA objective with 5% CO_2 and 37°C . Super-resolution experiments were acquired with the Zeiss LSM780 ELYRA. Images were processed for Structured Illumination with Zen software.

Electrophoresis and western blotting

Cell lysates were obtained with Laemmli buffer composed of 60 mM Tris-HCl pH 6.8, 10% glycerol, 2% SDS and 50 mM DTT with the addition of anti-protease (cOmplete cocktail, Roche 11 873 588 001), 1 mM glycerol phosphate, 1 mM sodium orthovanadate and 1 mM sodium fluoride. Samples were boiled 5 min at 95°C before loading on polyacrylamide gels. Transfer occurred at 100 V for 1 h on nitrocellulose membranes. Membranes were blotted with TBST (0.2% Tween) and 5% milk and incubated for 1 h with the primary antibody, followed by 1 h with HRP-conjugated secondary antibody. Bands were revealed with ECL chemoluminescent substrate (Pierce, Thermo Scientific or Bio-Rad).

Antibodies used were: anti- α -tubulin (1:500, MCA77G, Bio-Rad), anti-GAPDH (1:10,000, MAB374, Chemicon International), anti-acetylated tubulin (1:10,000, clone 6-11B-1, Sigma-Aldrich), anti-Rab6A (1:500, sc-310, Santa Cruz Biotechnology) and anti-Poly-Glu tubulin (1:1000, AbC0101, ValBiotech). Secondary antibodies were Alexa Fluor 488 donkey anti-rabbit (711-545-152), Rhodamine (TRITC) donkey anti-rabbit (711-025-152), Alexa Fluor 647 donkey anti-rabbit (711-695-152), Alexa Fluor 488 donkey anti-mouse (715-545-151), Rhodamine (TRITC) donkey anti-mouse (715-025-151), Alexa Fluor 647 donkey anti-goat (705-605-147), and Alexa Fluor 488 donkey anti-rat (712-545-153) and Alexa Fluor TRITC donkey anti-rat (712-025-153), all from Jackson ImmunoResearch and used at a 1:1000 dilution.

Quantifications of images and movies

Analysis of FA number, area and distribution was performed with a custom-designed macro in Fiji. Briefly, for each image FA contours were determined by thresholding the paxillin fluorescence channel and using the Analyse Particles plugin and a minimum size of $0.5 \mu\text{m}^2$.

To quantify FA dynamics, integrated fluorescent intensity of single FA was analysed over time. The turnover was defined as the time elapsed between the appearance (first frame) and the disappearance (last frame). Assembly was defined as the time between appearance and the peak or plateau of fluorescence intensity. The plateau was defined as the period during which the integrated fluorescence of FA was high and constant, and disassembly was defined as the time between the beginning of integrated fluorescence intensity decrease and disappearance of the FA.

Normalised mean intensity levels of acetylated and detyrosinated tubulin for immunofluorescence images are calculated as follows:

$$\text{Normalised acetyl or detyr tubulin level at a given time } t = \frac{[(\text{Mean acetyl or detyr tubulin intensity at } t) / (\text{Mean } \alpha\text{-tubulin intensity at } t)]}{[(\text{Mean acetyl or detyr tubulin intensity at } t_0) / (\text{Mean } \alpha\text{-tubulin intensity at } t_0)]} \quad (1)$$

Two regions of a cell – perinuclear and the cell front (leading edge of the protrusion) – were used to quantify acetylated tubulin levels over time

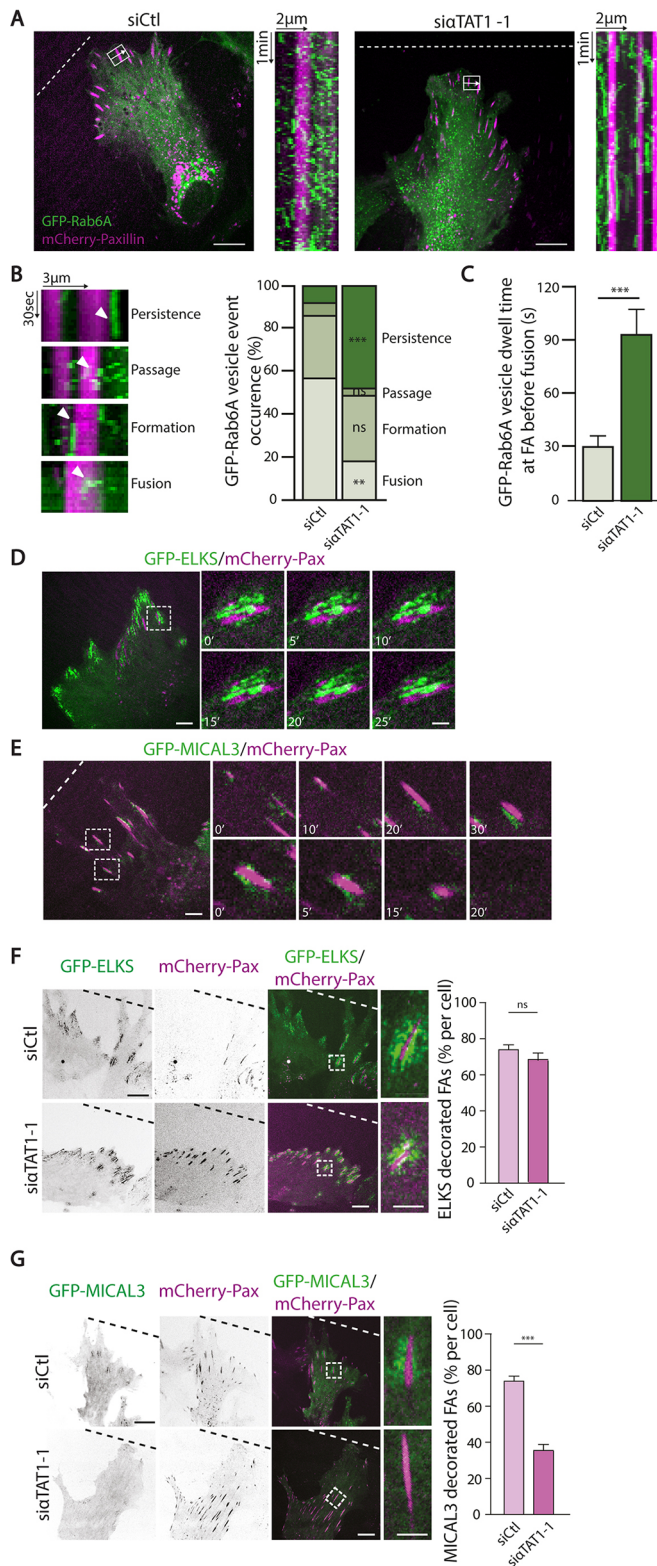


Fig. 4. α TAT1 controls Rab6A-positive vesicle fusion at focal adhesions. (A) Fluorescence images of migrating astrocytes transfected with indicated siRNAs, GFP-Rab6A (green) and mCherry-paxillin (magenta) (Movie 6). Dashed lines indicate wound orientation. Kymographs (to the right of each image) show the fluorescence intensity profile along the white arrow shown in the white box over time. (B) Graph showing the percentage of the different behaviours (persistence, passage, formation, fusion) of GFP-Rab6A-positive vesicles observed on the kymograph, as demonstrated in panel to the left. (C) Graph showing the mean \pm s.e.m. dwell time of GFP-Rab6A-positive vesicles at FAs before disappearance ($N=3$, 6 cells per experiment and >50 GFP-Rab6A-positive vesicles trajectories analysed). (D,E) Fluorescence images of migrating astrocytes transfected with mCherry-paxillin (magenta) and GFP-ELKS (green; D) or GFP-MICAL3 (green; E). Higher magnification images to the right show the localization and dynamics of GFP-ELKS (D) or GFP-MICAL3 (E) near FAs at indicated time points. (F,G) Fluorescent images of GFP-ELKS (green; F) or GFP-MICAL3 (green; G) and mCherry-paxillin (magenta) expressed in astrocytes transfected with control siRNA (siCtl) or si α TAT1-1. Higher magnification images in the far-right panels show the localization and dynamics of GFP-ELKS and GFP-MICAL3 near mCherry-paxillin. Graphs show mean \pm s.e.m. percentage of focal adhesions per cell decorated by ELKS (F) or MICAL3 (G) ($N=20$, number of cells).

cell nucleus,

$$v = \frac{\sum \vartheta}{n} \tag{2}$$

$$p = \frac{\sqrt{[(x_{24} - x_0)^2 + (y_{24} - y_0)^2]}}{\sum \sqrt{[(x_n - x_{n-1})^2 + (y_n - y_{n-1})^2]}} \tag{3}$$

$$d = \frac{(x_0 - x_{24})}{\sum \vartheta \sqrt{[(x_n - x_{n-1})^2 + (y_n - y_{n-1})^2]}} \tag{4}$$

where n is the number of time points acquired and ϑ is cell velocity.

For GFP-Rab6A-positive vesicle analysis (Fig. 4), ROIs of approximately 10–20 μm^2 around single FAs were drawn using MetaMorph (Molecular Devices). Areas were selected in the mCherry-paxillin channel independent of the GFP-Rab6A channel to not bias region selection. The image sequence was then cropped closely around FAs as indicated by the box in Fig. 4A. A sequence of x - t kymographs was generated with MetaMorph. The resulting image sequence is shown in the right-hand panel of Fig. 4A. GFP-Rab6A-positive vesicle events were separated in four categories. Fusion corresponds to the disappearance of the GFP-Rab6A-positive vesicle that stop moving close to the FAs. Persistence corresponds to GFP-Rab6A-positive vesicles that do not immediately disappear but remain close to the FAs before disappearing. Note that persistence of vesicles in the proximity of FAs is only observed in α TAT1-depleted cells. Formation corresponds to the appearance of the vesicle close to the FAs and passage corresponds to a GFP-Rab6A-positive vesicle moving across FAs. GFP-Rab6A-positive vesicle dwell time was defined as the persistence time of a vesicle before fusion and was measured as the length of vertical GFP-Rab6A tracks in the kymographs. GFP-Rab6A-positive vesicle behaviour and dwell-time were quantified. $n > 50$ FAs from three independent experiments (6 cells per experiment and >50 GFP-Rab6A-positive vesicles trajectories analysed). Statistical differences were determined using Student's t -test for GFP-Rab6A-positive vesicle dwell time and a χ^2 test by contingency for the percentage of vesicle events.

For the association of Rab6 with acetylated tubulin and total tubulin (Fig. S3C), the acetyl tubulin and total tubulin channels were thresholded and segmented. Masks of the segmented images were transferred onto the Rab6 channel, in order to measure the mean fluorescent intensities of Rab6 in association with acetylated or total tubulin microtubules. A linear fit was generated using GraphPad Prism 6.0.

Statistical analysis

The box-and-whisker plots show median, first and third quartiles (boxes), whiskers extending to the furthest observations.

during migration in different regions. A segmented line tool was used to draw a line (width 50 pixels) in front of the nucleus or at the cell edge as shown in the schematic (Fig. 3B). Acetylated tubulin and total tubulin intensities in these regions were measured and a normalized acetyl level for each region was calculated using the equation above.

Mean velocity (v), persistence (p) and directionality (d) of cell migration are calculated as follows: for a given x,y coordinate of leading

N-values indicate the number of independent experiments. Statistical analysis was obtained using Student's *t*-test (Fig. 2H) or one-way ANOVA (all figures except Fig. 2H) followed by Tukey's multiple comparisons post-hoc test. Analyses were performed with GraphPad Prism 5.0 or 6.0. *P*-values are reported as n.s. (not significant) for $P > 0.05$, * $P < 0.05$, ** $P < 0.01$, *** $P < 0.001$ and **** $P < 0.0001$.

Acknowledgements

We would like to thank members of the Etienne-Manneville lab for support and discussion, as well as Jean-Baptiste Manneville for stimulating discussion and careful reading of the manuscript. We thank A. M. Vallés (Institut Curie), Carsten Janke (Institut Curie), Bruno Goud, (Institut Curie), Anna Akhmanova (Utrecht University, Netherlands) and Philippe Chavrier (Institut Curie) for reagents and helpful discussions. We gratefully acknowledge Jean Yves Tinevez and Audrey Salles and the Imagopole of Institut Pasteur (Paris, France) as well as the France-BioImaging infrastructure network supported by the French National Research Agency (ANR-10-INSB-04; Investments for the Future) and the Région Ile-de-France (program Domaine d'Intérêt Majeur-Malin) for the use of the Elyra microscope.

Competing interests

The authors declare no competing or financial interests.

Author contributions

Conceptualization: S.E.-M.; Methodology: B. Bance, S.S., C.L., B. Boeda, S.E.-M.; Validation: S.E.-M.; Formal analysis: B. Bance, S.S., S.E.-M.; Investigation: B. Bance, S.S.; Resources: S.E.-M.; Data curation: B. Bance, S.S., C.L., S.E.-M.; Writing - original draft: S.E.-M.; Writing - review & editing: B. Bance, S.S., C.L., B. Boeda, S.E.-M.; Visualization: C.L.; Supervision: B. Boeda, S.E.-M.; Project administration: S.E.-M.; Funding acquisition: S.E.-M.

Funding

This work was supported by the Ligue Contre le Cancer, the Centre National de la Recherche Scientifique and the Institut Pasteur. B. Bance was funded by Ligue Contre le Cancer. S.S. is funded by the ITN PolarNet Marie Skłodowska-Curie grant and is part of the Ecole Doctorale Frontières du Vivant (FdV) – Programme Bettencourt. B. Boeda is a full-time INSERM researcher at the CNRS.

Supplementary information

Supplementary information available online at <http://jcs.biologists.org/lookup/doi/10.1242/jcs.225805.supplemental>

References

- Aillaud, C., Bosc, C., Saoudi, Y., Denarier, E., Peris, L., Sago, L., Taulet, N., Cieren, A., Tort, O., Magiera, M. M. et al. (2016). Evidence for new C-terminally truncated variants of alpha- and beta-tubulins. *Mol. Biol. Cell* **27**, 640-653.
- Aillaud, C., Bosc, C., Peris, L., Bosson, A., Heemeryck, P., Van Dijk, J., Le Friec, J., Boulan, B., Vossier, F., Sanman, L. E. et al. (2017). Vasohibins/SVBP are tubulin carboxypeptidases (TCPs) that regulate neuron differentiation. *Science* **358**, 1448-1453.
- Akella, J. S., Wloga, D., Kim, J., Starostina, N. G., Lyons-Abbott, S., Morrissette, N. S., Dougan, S. T., Kipreos, E. T. and Gaertig, J. (2010). MEC-17 is an alpha-tubulin acetyltransferase. *Nature* **467**, 218-222.
- Bretscher, M. S. and Aguado-Velasco, C. (1998). Membrane traffic during cell locomotion. *Curr. Opin. Cell Biol.* **10**, 537-541.
- Castro-Castro, A., Janke, C., Montagnac, G., Paul-Gilloteaux, P. and Chavrier, P. (2012). ATAT1/MEC-17 acetyltransferase and HDAC6 deacetylase control a balance of acetylation of alpha-tubulin and cortactin and regulate MT1-MMP trafficking and breast tumor cell invasion. *Eur. J. Cell Biol.* **91**, 950-960.
- Cook, T. A., Nagasaki, T. and Gundersen, G. G. (1998). Rho guanine triphosphatase mediates the selective stabilization of microtubules induced by lysophosphatidic acid. *J. Cell Biol.* **141**, 175-185.
- Creppe, C., Malinowskaya, L., Volvert, M.-L., Gillard, M., Close, P., Malaise, O., Laguesse, S., Cornez, I., Rahmouni, S., Ormenese, S. et al. (2009). Elongator controls the migration and differentiation of cortical neurons through acetylation of alpha-tubulin. *Cell* **136**, 551-564.
- Digman, M. A., Brown, C. M., Horwitz, A. R., Mantulin, W. W. and Gratton, E. (2008). Paxillin dynamics measured during adhesion assembly and disassembly by correlation spectroscopy. *Biophys. J.* **94**, 2819-2831.
- Eric, J. and Etienne-Manneville, S. (2014). Centrosome positioning in polarized cells: common themes and variations. *Exp. Cell Res.* **328**, 240-248.
- Etienne-Manneville, S. (2004). Actin and microtubules in cell motility: which one is in control? *Traffic* **5**, 470-477.
- Etienne-Manneville, S. (2006). In vitro assay of primary astrocyte migration as a tool to study Rho GTPase function in cell polarization. *Methods Enzymol.* **406**, 565-578.
- Etienne-Manneville, S. (2010). From signaling pathways to microtubule dynamics: the key players. *Curr. Opin. Cell Biol.* **22**, 104-111.
- Etienne-Manneville, S. (2013). Microtubules in cell migration. *Annu. Rev. Cell Dev. Biol.* **29**, 471-499.
- Etienne-Manneville, S. and Hall, A. (2001). Integrin-mediated activation of Cdc42 controls cell polarity in migrating astrocytes through PKCzeta. *Cell* **106**, 489-498.
- Ezraty, E. J., Partridge, M. A. and Gundersen, G. G. (2005). Microtubule-induced focal adhesion disassembly is mediated by dynamin and focal adhesion kinase. *Nat. Cell Biol.* **7**, 581-590.
- Ezraty, E. J., Bertaux, C., Marcantonio, E. E. and Gundersen, G. G. (2009). Clathrin mediates integrin endocytosis for focal adhesion disassembly in migrating cells. *J. Cell Biol.* **187**, 733-747.
- Fourriere, L., Kasri, A., Gareil, N., Bardin, S., Boulanger, J., Sikora, R., Boncompain, G., Miserey-Lenkei, S., Perez, F. and Goud, B. (2018). RAB6 and microtubules restrict secretion to focal adhesions. *bioRxiv*, 382176.
- Gadadhar, S., Bodakuntla, S., Natarajan, K. and Janke, C. (2017). The tubulin code at a glance. *J. Cell Sci.* **130**, 1347-1353.
- Gao, Y.-S., Hubbert, C. C., Lu, J., Lee, Y.-S., Lee, J.-Y. and Yao, T.-P. (2007). Histone deacetylase 6 regulates growth factor-induced actin remodeling and endocytosis. *Mol. Cell Biol.* **27**, 8637-8647.
- Gardel, M. L., Schneider, I. C., Aratyn-Schaus, Y. and Waterman, C. M. (2010). Mechanical integration of actin and adhesion dynamics in cell migration. *Annu. Rev. Cell Dev. Biol.* **26**, 315-333.
- Goud, B., Yang, C., Roa, M., Martinez, O. and Slepnev, V. (1994). Study of rab6, a ras-like GTP-binding protein associated with the Golgi complex. *Ann. N.Y. Acad. Sci.* **733**, 340-343.
- Grigoriev, I., Splinter, D., Keijzer, N., Wulf, P. S., Demmers, J., Ohtsuka, T., Modesti, M., Maly, I. V., Grosveld, F., Hoogenraad, C. C. et al. (2007). Rab6 regulates transport and targeting of exocytotic carriers. *Dev. Cell* **13**, 305-314.
- Grigoriev, I., Yu, K. L., Martinez-Sanchez, E., Serra-Marques, A., Smal, I., Meijering, E., Demmers, J., Peränen, J., Pasterkamp, R. J., Van Der Sluijs, P. et al. (2011). Rab6, Rab8, and MICAL3 cooperate in controlling docking and fusion of exocytotic carriers. *Curr. Biol.* **21**, 967-974.
- Gundersen, G. G. and Bulinski, J. C. (1988). Selective stabilization of microtubules oriented toward the direction of cell migration. *Proc. Natl. Acad. Sci. USA* **85**, 5946-5950.
- Haggarty, S. J., Koeller, K. M., Wong, J. C., Grozinger, C. M. and Schreiber, S. L. (2003). Domain-selective small-molecule inhibitor of histone deacetylase 6 (HDAC6)-mediated tubulin deacetylation. *Proc. Natl. Acad. Sci. USA* **100**, 4389-4394.
- Hubbert, C., Guardiola, A., Shao, R., Kawaguchi, Y., Ito, A., Nixon, A., Yoshida, M., Wang, X.-F. and Yao, T.-P. (2002). HDAC6 is a microtubule-associated deacetylase. *Nature* **417**, 455-458.
- Janke, C. (2014). The tubulin code: molecular components, readout mechanisms, and functions. *J. Cell Biol.* **206**, 461-472.
- Kalebic, N., Martinez, C., Perlas, E., Hublitz, P., Bilbao-Cortes, D., Fiedorczuk, K., Andolfo, A. and Heppenstall, P. A. (2013a). Tubulin acetyltransferase alphaTAT1 destabilizes microtubules independently of its acetylation activity. *Mol. Cell Biol.* **33**, 1114-1123.
- Kalebic, N., Sorrentino, S., Perlas, E., Bolasco, G., Martinez, C. and Heppenstall, P. A. (2013b). alphaTAT1 is the major alpha-tubulin acetyltransferase in mice. *Nat. Commun.* **4**, 1962.
- Kaverina, I., Rottner, K. and Small, J. V. (1998). Targeting, capture, and stabilization of microtubules at early focal adhesions. *J. Cell Biol.* **142**, 181-190.
- Kaverina, I., Krylyshkina, O. and Small, J. V. (1999). Microtubule targeting of substrate contacts promotes their relaxation and dissociation. *J. Cell Biol.* **146**, 1033-1044.
- Kaverina, I., Krylyshkina, O. and Small, J. V. (2002). Regulation of substrate adhesion dynamics during cell motility. *Int. J. Biochem. Cell Biol.* **34**, 746-761.
- Kim, G.-W., Li, L., Gorbani, M., You, L. and Yang, X.-J. (2013). Mice lacking alpha-tubulin acetyltransferase 1 are viable but display alpha-tubulin acetylation deficiency and dentate gyrus distortion. *J. Biol. Chem.* **288**, 20334-20350.
- Kovacs, J. J., Murphy, P. J. M., Gaillard, S., Zhao, X., Wu, J.-T., Nicchitta, C. V., Yoshida, M., Toft, D. O., Pratt, W. B. and Yao, T.-P. (2005). HDAC6 regulates Hsp90 acetylation and chaperone-dependent activation of glucocorticoid receptor. *Mol. Cell* **18**, 601-607.
- Li, L. and Yang, X.-J. (2015). Tubulin acetylation: responsible enzymes, biological functions and human diseases. *Cell Mol. Life Sci.* **72**, 4237-4255.
- Llense, F. and Etienne-Manneville, S. (2015). Front-to-rear polarity in migrating cells. In *Cell Polarity*. (ed. K. Ebneth), pp. 115-146. Springer.
- Montagnac, G., Meas-Yedid, V., Irontelle, M., Castro-Castro, A., Franco, M., Shida, T., Nachury, M. V., Benmerah, A., Olivo-Marin, J.-C. and Chavrier, P. (2013). alphaTAT1 catalyses microtubule acetylation at clathrin-coated pits. *Nature* **502**, 567-570.
- Palazzo, A. F., Eng, C. H., Schlaepfer, D. D., Marcantonio, E. E. and Gundersen, G. G. (2004). Localized stabilization of microtubules by integrin- and FAK-facilitated Rho signaling. *Science* **303**, 836-839.

- Parsons, J. T., Horwitz, A. R. and Schwartz, M. A.** (2010). Cell adhesion: integrating cytoskeletal dynamics and cellular tension. *Nat. Rev. Mol. Cell Biol.* **11**, 633-643.
- Raunser, S. and Gatsogiannis, C.** (2015). Deciphering the tubulin code. *Cell* **161**, 960-961.
- Shafaq-Zadah, M., Gomes-Santos, C. S., Bardin, S., Maiuri, P., Maurin, M., Iranzo, J., Gautreau, A., Lamaze, C., Caswell, P., Goud, B. et al.** (2016). Persistent cell migration and adhesion rely on retrograde transport of beta(1) integrin. *Nat. Cell Biol.* **18**, 54-64.
- Song, Y. and Brady, S. T.** (2015). Post-translational modifications of tubulin: pathways to functional diversity of microtubules. *Trends Cell Biol.* **25**, 125-136.
- Stehbens, S. and Wittmann, T.** (2012). Targeting and transport: how microtubules control focal adhesion dynamics. *J. Cell Biol.* **198**, 481-489.
- Stehbens, S. J., Paszek, M., Pemble, H., Ettinger, A., Gierke, S. and Wittmann, T.** (2014). CLASPs link focal-adhesion-associated microtubule capture to localized exocytosis and adhesion site turnover. *Nat. Cell Biol.* **16**, 558-570.
- Strzyz, P.** (2016). Post-translational modifications: Extension of the tubulin code. *Nat. Rev. Mol. Cell Biol.* **17**, 609.
- Tran, A. D.-A., Marmo, T. P., Salam, A. A., Che, S., Finkelstein, E., Kabarriti, R., Xenias, H. S., Mazitschek, R., Hubbert, C., Kawaguchi, Y. et al.** (2007). HDAC6 deacetylation of tubulin modulates dynamics of cellular adhesions. *J. Cell Sci.* **120**, 1469-1479.
- Webb, D. J., Donais, K., Whitmore, L. A., Thomas, S. M., Turner, C. E., Parsons, J. T. and Horwitz, A. F.** (2004). FAK-Src signalling through paxillin, ERK and MLCK regulates adhesion disassembly. *Nat. Cell Biol.* **6**, 154-161.
- Wolfenson, H., Henis, Y. I., Geiger, B. and Bershadsky, A. D.** (2009). The heel and toe of the cell's foot: a multifaceted approach for understanding the structure and dynamics of focal adhesions. *Cell Motil. Cytoskeleton* **66**, 1017-1029.
- Yu, I., Garnham, C. P. and Roll-Mecak, A.** (2015). Writing and reading the tubulin code. *J. Biol. Chem.* **290**, 17163-17172.
- Zhang, X., Yuan, Z., Zhang, Y., Yong, S., Salas-Burgos, A., Koomen, J., Olashaw, N., Parsons, J. T., Yang, X. J., Dent, S. R. et al.** (2007). HDAC6 modulates cell motility by altering the acetylation level of cortactin. *Mol. Cell* **27**, 197-213.